Influence of dosimetry method on bone lesion absorbed dose estimates in PSMA therapy: application to mCRPC patients receiving Lu-177-PSMA-I&T

Julia Brosch (julia.brosch@med.uni-muenchen.de)
University Hospital, LMU Munich https://orcid.org/0000-0002-5680-5823
Carlos Uribe
BC Cancer; University of British Columbia
Astrid Gosewisch
University Hospital, LMU Munich
Lena Kaiser
University Hospital, LMU Munich
Andrei Todica
University Hospital, LMU Munich
Harun Ilhan
University Hospital, LMU Munich
Franz Josef Gildehaus
University Hospital, LMU Munich
Peter Bartenstein
University Hospital, LMU Munich
Arman Rahmim
BC Cancer; University of British Columbia
Anna Celler
University of British Columbia
Sibylle Ziegler
University Hospital, LMU Munich
Guido Böning
University Hospital, LMU Munich

Original research

Keywords: Radioligand therapy, mCRPC, PSMA, Lutetium-177, 3D dosimetry, tumor dosimetry, OLINDA/EXM®, voxel S value, Monte Carlo simulation

Posted Date: August 3rd, 2020

DOI: https://doi.org/10.21203/rs.3.rs-50788/v1

Influence of dosimetry method on bone lesion absorbed dose estimates in PSMA therapy: application to mCRPC patients receiving Lu-177-PSMA-I&T

Julia Brosch[1], Carlos Uribe[2,3], Astrid Gosewisch[1], Lena Kaiser[1], Andrei Todica[1], Harun Ilhan[1], Franz Josef Gildehaus[1], Peter Bartenstein[1], Arman Rahmim[2,3,4], Anna Celler[3], Sibylle Ziegler[1], Guido Böning[1,*]

[1]Department of Nuclear Medicine, University Hospital, LMU Munich; Marchioninistrasse 15, 81377 Munich, Germany

[2]PET Functional Imaging, BC Cancer, 600 West 10th Avenue, Vancouver, BC, V5Z 4E6, Canada

[3]Department of Radiology, University of British Columbia, 2775 Laurel Street, Vancouver, BC, V5Z 1M9, Canada

[4]Department of Integrative Oncology, BC Cancer Research Centre, 675 West 10th Avenue, Vancouver, BC, V5Z 1L3, Canada

Julia Brosch: Julia.Brosch@med.uni-muenchen.de

Carlos Uribe: curibe@bccrc.ca

Astrid Gosewisch: Astrid.Gosewisch@med.uni-muenchen.de

Lena Kaiser: Lena.Kaiser@med.uni-muenchen.de

Andrei Todica: Andrei.Todica@med.uni-muenchen.de

Harun Ilhan: Harun.Ilhan@med.uni-muenchen.de

Franz Josef Gildehaus: Franz.Gildehaus@med.uni-muenchen.de

Peter Bartenstein: Peter.Bartenstein@med.uni-muenchen.de

Arman Rahmim: arman.rahmim@ubc.ca

Anna Celler: aceller@phas.ubc.ca

Sibylle Ziegler: Sibylle.Ziegler@med.uni-muenchen.de

Guido Böning: Guido.Boening@med.uni-muenchen.de

***Correspondence should be addressed to**

Julia Brosch

Abstract

Background

Patients with metastatic, castration-resistant prostate cancer (mCRPC) present with an increased tumor burden in the skeleton. For these patients, Lutetium-177 (Lu-177) radioligand therapy targeting the prostate-specific membrane antigen (PSMA) has gained increasing interest with promising outcome data. Patient-individualized dosimetry enables quantification of therapy success with the aim of minimizing absorbed dose to organs at risk while maximizing absorbed dose to tumors. Different dosimetric approaches with varying complexity and accuracy exist for this purpose. The relatively simple OLINDA method applied to tumors assumes a homogeneous activity distribution in a sphere with unit density. Voxel S value (VSV) approaches can account for heterogeneous activities but are simulated for a specific tissue. Full patient-individual Monte Carlo (MC) dose simulation addresses both, heterogeneous activity and density distributions. Subsequent CT-based density correction has the potential to overcome the assumption of homogeneous density in OLINDA and VSV methods, which could be a major limitation for the application in bone metastases with heterogeneous density. The aim of this investigation is a comparison of these methods for bone lesion dosimetry in mCRPC patients receiving Lu-177-PSMA therapy.

Results

In total, 289 bone lesions in 15 mCRPC patients were analyzed. Percentage deviation (PD) of absorbed lesion doses compared to full MC was +7 ±13 % (min: -60 %; max: +47 %) for the OLINDA unit density sphere model. With an applied CT-based density weighting to account for density differences in bone lesions, PD was -15 ±6 % (min: -54 %; max: -2 %). For a soft tissue VSV approach, large PDs of +16 ±13 % (min: -56 %; max: +57 %) were found; after voxel-wise density correction this was reduced to -5 ±2 % (min: -15 %; max: -2 %). The use of a combination of standard soft tissue and cortical bone VSVs showed deviations of -35 ±8 % (min: -76 %; max: +5 %). With additional voxel-wise density weighting, the PD was -3 ±2 % (min: -13 %; max: 0 %).

Conclusion

Based on our bone lesion dosimetry results, a VSV approach with subsequent CT-based, voxel-wise density correction enabled dose estimates, that closely replicate computationally-demanding gold-standard full MC dose simulations.

Keywords

Radioligand therapy, mCRPC, PSMA, Lutetium-177, 3D dosimetry, tumor dosimetry, OLINDA/EXM®, voxel S value, Monte Carlo simulation

Background

The incidence of prostate cancer has been steadily increasing over the past decades in western populations (1, 2). Patients with castration-resistant prostate cancer (mCRPC) typically present a large metastatic tumor burden in the bones (3). Radioligand therapies (RLT) targeting the prostate-specific membrane antigen (PSMA) such as Lutetium-177-PSMA (Lu-177-PSMA) and Actinium-225-PSMA have shown promising results in patients ineligible for other therapies or showing progress after receiving other systemic treatment options (4). The clinical value of personalized dosimetry in RLT lies in a possible increase of the therapeutic window by limiting absorbed dose to organs at risk (OARs) while maximizing absorbed dose to tumors. Thus, personalized dosimetry is indispensable for correlation with therapy response and patient outcome and enables adjustments for subsequent therapy cycles. First Lu-177-DKFZ-PSMA-617 absorbed dose estimates were published in 2015 (5). Nonetheless, up to now there are still few publications addressing the absorbed doses delivered to tumors after Lu-177-PSMA therapy (5-11). There are different approaches for calculation of absorbed doses, each with varying complexity and accuracy. The use of pre-calculated organ specific S values has become more prevalent using the OLINDA/EXM® 2.0 software (HERMES Medical Solutions, Sweden) (12). However, this approach relies on the unit density sphere model for calculation of tumor S values that assumes homogeneous activity distribution within the tumor and a tumor density of 1 g/cm^3 (i.e. soft tissue). Thus, this fast and simple approach has limited applicability to bone lesions with higher densities and non-uniform activity distributions. An alternative dosimetry approach includes radionuclide specific dose kernels or voxel S values (VSVs), which are pre-simulated for a specific tissue type and voxel size. The use of VSVs enables a three-dimensional (3D) absorbed dose calculation and is capable to account for heterogeneous activity distributions under the assumption of a homogeneous material and density (13). The inherent complexity of Monte Carlo (MC) absorbed dose simulations makes this technique superior in addressing patient-individual heterogeneous density and activity distributions for a 3D absorbed dose calculation. However, the

majority of publications reporting tumor absorbed dose estimates in Lu-177-PSMA therapies use the OLINDA unit density sphere model approach (5-7, 9-11).

The aim of this work is to provide further insight into various dosimetry techniques especially for accurate and reproducible bone lesion dose estimation in Lu-177-PSMA therapy of mCRPC. The methods being investigated for this purpose made use of the OLINDA unit density sphere model for VOI-based dosimetry, VSVs for different tissue types for voxel-based dosimetry, and were extended by considering a tissue-specific density weighting approach. Their capability of absorbed dose quantification was evaluated in comparison to patient-individual dosimetry by Monte Carlo simulations. The latter is assumed to be the most accurate and is referred to as the gold-standard approach.

Methods

Patients

The study was conducted retrospectively on anonymized data and was approved by the local ethics committee of our institution. 15 patients with metastatic, castration-resistant prostate cancer (mCRPC) and pronounced metastases in the skeleton were included in this study. Table 1 presents the detailed patient characteristics. Patients received a first cycle of radioligand therapy using Lu-177-PSMA-I&T with activities of 7.45 ± 0.02 GBq in 10 patients and 9.06 ± 0.06 GBq in 5 patients. The higher initial therapy activities were used in case of severe bone metastasis and/or presence of visceral metastasis.

Image acquisition and reconstruction

Following the standard clinical routine imaging protocol of our institution, patients underwent quantitative Lu-177 SPECT/CT imaging (Symbia Intevo^{TM} T16 SPECT/CT, 3/8” crystal, medium-energy low-penetration collimator, Siemens Healthcare, Germany) at 24 h, 48 h and 72 h post injection (p.i.). At least two SPECT bed positions were acquired in auto-contour mode followed by a low dose CT.

Image acquisition parameters included a 128x128 matrix with 64 angular steps and a duration of 5 s per step. The imaging energy window was centered at the energy of the upper photo peak of Lu-177 at 208 keV (width 15 %). Quantitative SPECT reconstruction was performed with collimator-specific depth-dependent detector response modelling, corrections for photon attenuation and scattering and using a system-specific calibration factor (16 MAP iterations, 8 subsets, Bayesian weight 0.01, Hermes Hybrid Recon v.2.1.1, HERMES Medical Solutions, Sweden) (14, 15).

Image processing

All images were processed with PMOD (v4.005; PMOD Technologies LLC). Rigid co-registration of all CT and SPECT volumes was performed onto the SPECT/CT image data at 24 h p.i., which served as reference. An individual bone map and a whole-body volume of interest (VOI) were derived from the reference CT by threshold-based segmentation, and kidney VOIs were defined by manual delineation. To further segment individual bone lesions within the skeletal bone map, the semi-automatic k-means cluster segmentation of PMOD 3D tool was used on the 24 h SPECT (3). All VOIs were copied to the co-registered SPECT data sets. VOI activities for whole-body, kidneys and tumor lesions were fitted using a mono-exponential fit model to acquire the effective half-lives per VOI. Time-integrated activity images per patient were consequently generated with MATLAB (R2019b, The MathWorks, Inc. Natick, MA) based on the reference SPECT at 24 h p.i. and the individual VOI map:

$$\tilde{A}^{voxel} = \frac{A_{t=0}^{voxel}}{\lambda_{VOI}}, \quad (1)$$

where $\tilde{A}^{voxel}$ denotes the time-integrated activity per voxel, $A_{t=0}^{voxel}$ is the activity at time point zero in a voxel, and λ_{VOI} equal to ln(2) divided by the effective half-life obtained from mono-exponential fitting in the related VOI. $A_{t=0}^{voxel}$ was computed as:

$$A_{t=0}^{voxel} = A_{t=24\,h}^{voxel} \cdot e^{\lambda_{VOI} \cdot t(t=24\,h)}. \quad (2)$$

Dosimetry calculations

We investigated 7 different dosimetry approaches by utilizing the aforementioned time-integrated activity images and the reference CT of each patient, and evaluated them based on their accuracy (with respect to Monte Carlo), complexity, and feasibility to integrate into clinical practice.

1) MC method: Patient-specific Monte Carlo (MC) dose simulation

Patient-specific MC dose simulation accounts for the patient's anatomy by using the geometry and density information from the patient's CT image (16). The radioactive decay, the interactions of the radioactive decay products with matter and consequently the absorbed dose deposition are simulated based on the patient-individual time-integrated activity distribution. Hence, MC dose simulations contain the highest level of complexity for modelling the physical processes for dose estimation amongst all other applied methods in this study and are considered the gold-standard for dosimetry. In concordance with Dieudonné et al. (17) and Grimes et al. (18), we considered MC dosimetry as the reference method assessing the suitability and accuracy of the other methods for bone lesion dosimetry. Monte Carlo simulations in this study were performed using the GATE MC code version 8.2, based on GEANT4 version 10.5.1. This code has previously been validated for use in nuclear medicine therapies (19-21). In detail, Hounsfield Units (HU) of patients' CT data were converted into material compositions and densities according to Schneider et al. (16), giving a HU to density conversion table. The time-integrated activity image of each patient was normalized with its total number of decays and used as the input for the simulations. The total number of 10^9 primary decays per patient simulation was divided into 20 sub-simulations for parallel execution on separate CPUs to increase simulation speed. The relative statistical uncertainty in the absorbed dose per voxel was calculated as described by Chetty et al. (22). The voxel size of the simulation was $(4.7952\ \text{mm})^3$ corresponding to the voxel sizes of the SPECT acquisitions. All particle range thresholds were set to 0.1 mm.

2) OLINDA method: OLINDA unit density sphere model

The OLINDA uniform and unit density sphere model (OLINDA/EXM® 2.0, HERMES Medical Solutions, Sweden) represents the model with the lowest level of complexity and can be considered as the most simple and applicable method, yet clinically available. Since the total time-integrated activity per lesion and the lesion volume were known from the processing steps described above, the mean lesion absorbed dose was calculated following the Medical Internal Radiation Dose (MIRD) Committee formalism (23) by multiplication of the OLINDA S value for the selected tumor volume with the tumor time-integrated activity. OLINDA S values are available for a limited number of sphere volumes/masses. Hence, the appropriate OLINDA S value per lesion was obtained by fitting the available OLINDA S values and subsequent calculation of the S value for the lesion mass with the fit parameters assuming the lesion mass being equal to the lesion volume expressing a unit density. This method includes solely the tumor self-dose (24) and is further based on the assumption that tumors and lesions were all of spherical shape with unit density and uniform activity distribution (12).

3) OLINDA$_{weighted}$ method: OLINDA unit density sphere model with additional density weighting

As stated above, the unit density sphere model does not only neglect the actual tumor shape but also the actual tumor density. A simple method aiming to improve this dose estimate and to account for the tissue-specific tumor density is to convert the average HU from the lesion VOI on the CT-image to an average lesion density using the HU to density conversion table and to adjust the dose estimate. This was achieved by weighting the lesion absorbed dose value D^{lesion} with the ratio of unit density by the average lesion density ρ_{lesion} according to:

$$D_{weighted}^{lesion} = D^{lesion} \cdot \frac{1\,{}^{g}/_{ccm}}{\rho_{lesion}}. \quad (3)$$

4) VSV^{soft} method: Dose convolution model using voxel S values (VSVs) based on ICRP soft tissue

The OLINDA methods assume uniform distributions of activity within organs and tumors neglecting the heterogeneous distributions that are observed in SPECT images. To account for the non-uniform activity distribution in 3D dosimetry, the use of VSVs for dosimetry has gained increasing interest (13). For this purpose, GATE MC code was used for the simulation of Lu-177 VSVs using the voxel size

of the time-integrated activity images, namely (4.7952 mm)³. The simulation used the soft tissue composition according to the International Commission On Radiological Protection (ICRP) (25, 26). For simulation, the central voxel of the ICRP soft tissue medium in a 51 x 51 x 51 matrix was set as Lu-177 source voxel and 10^8 primaries were simulated. All particle range threshold were set to 0.1 mm. The VSVs represent the dose distribution per decay such that when convolved with the time-integrated activity image this results in a patient-specific 3D voxel dose map.

5) $VSV^{soft}_{weighted}$ method: Dose convolution model using VSVs based on ICRP soft tissue with additional density weighting

A limitation of the VSV^{soft} method was that the VSVs were simulated exclusively for soft tissue, and hence the applicability for bone lesion dosimetry is hindered.

Similar to the density weighting presented in the $OLINDA_{weighted}$ method, it is possible to adjust for the different densities of the patient-individual anatomy and the density of the simulated VSVs. For this, the HUs of the patients' CT were voxel-wise converted into density values, giving a density map. Consequently, the 3D absorbed dose map from the VSV^{soft} method is voxel-wise weighted with the ratio of the VSV density of ICRP soft tissue ρ_{ICRP} to the actual voxel density ρ_{voxel} (17):

$$D^{voxel}_{weighted} = D^{voxel} \cdot \frac{\rho_{ICRP}}{\rho_{voxel}}. \quad (4)$$

6) $VSV^{soft+bone}$ method: Dose convolution model using VSVs based on ICRP soft tissue and VSVs based on ICRP cortical bone

We extended the VSV^{soft} method by simulation of cortical bone VSVs using a standard ICRP cortical bone composition (25, 26) with a similar simulation setup as for the ICRP soft tissue VSVs in the VSV^{soft} method. Making use of the patient's bone map to distinguish between regions containing bone or soft tissue, the corresponding tissue-specific VSVs were applied in their respective regions similar to Lee et al. (27). Subsequently, to obtain a total 3D voxel dose map, the soft tissue 3D voxel

dose map (in soft tissue regions) and the cortical bone 3D voxel dose map (in bone regions) are combined into a single image.

7) $VSV^{soft+bone}_{weighted}$ method: Dose convolution model using VSVs based on ICRP soft tissue and VSVs based on ICRP cortical bone with additional density weighting

The skeleton itself is not merely composed of cortical bone, and shows a heterogeneous composition of tissues with varying densities. Therefore, to further account for the variations in bone composition, beyond the above-mentioned standard cortical model, a similar voxel-wise density weighting as in equation (4) is applied to the obtained combined 3D absorbed voxel dose map from the $VSV^{soft+bone}$ method in order to correct for differences in density per voxel.

Comparisons

To evaluate the 3D voxel dose maps obtained from MC, VSV^{soft}, $VSV^{soft}_{weighted}$, $VSV^{soft+bone}$ and $VSV^{soft+bone}_{weighted}$, VOIs from the initial bone lesion segmentation were utilized to quantify lesion absorbed dose estimates.

For objective assessment of quantification quality, the percentage difference PD of the mean absorbed dose per lesion of $\bar{D}^{lesion}_{method}$ obtained from the methods (OLINDA, $OLINDA_{weighted}$, VSV^{soft}, $VSV^{soft}_{weighted}$, $VSV^{soft+bone}$ and $VSV^{soft+bone}_{weighted}$) were compared with the mean absorbed dose per lesion obtained from MC $\bar{D}^{lesion}_{MC}$:

$$PD = \frac{\bar{D}^{lesion}_{method} - \bar{D}^{lesion}_{MC}}{\bar{D}^{lesion}_{MC}} \cdot 100. \quad (5)$$

Further comparison was performed by MATLAB Pearson's correlation and by Bland-Altman plots (28).

Cumulative dose volume histograms (DVHs) were created for the 3D dose methods for some exemplarily chosen lesions to enable a dose distribution comparison of the methods.

Results

In total, 289 bone lesions in the 15 mCRPC patients were evaluated. The segmented lesion volumes were on average 19.1 ml (range: 1.1 to 453.2 ml).

MC simulations

The overall simulation time per patient for the MC method was less than 4.5 h using the 20 parallel running MC sub-simulations. The maximum relative statistical uncertainty in absorbed dose simulations was below 2.4 % for all voxels in all lesions, with on average being below 0.9 % over all lesion voxels. The maximum statistical uncertainty in the absorbed dose for the target region of ICRP soft tissue and ICRP cortical bone VSVs of the VSV^{soft}, $VSV^{soft}_{weighted}$, $VSV^{soft+bone}$ and $VSV^{soft+bone}_{weighted}$ methods was below 3.2 %. This was for the most distant voxel from the source voxel. The average over all target voxels was below 2.0 %.

Comparison of dosimetry methods

The mean percentage difference (PD) of lesion absorbed dose estimates for each of the methods compared to full MC simulation based dose estimate, averaged over all investigated lesions, are summarized in Table 2. $VSV^{soft+bone}_{weighted}$ showed the smallest percentage deviation of -3 ±2 % accompanied with a relatively small range between the minimum percentage deviation of -13 % and maximum percentage deviation of 0 %. The additional density weighting of $OLINDA_{weighted}$, $VSV^{soft}_{weighted}$, and $VSV^{soft+bone}_{weighted}$, led to an overall smaller range of percentage deviations than the associated method without weighting, which is illustrated in Figure 1.

A very strong correlation with the MC absorbed dose estimates was found for all methods: OLINDA ($r = 0.982$, $p << 0.001$, $R^2 = 0.965$), $OLINDA_{weighted}$ ($r = 0.994$, $p << 0.001$, $R^2 = 0.988$), VSV^{soft} ($r = 0.983$, $p << 0.001$, $R^2 = 0.967$), $VSV^{soft}_{weighted}$ ($r = 1.000$, $p << 0.001$, $R^2 = 0.999$), $VSV^{soft+bone}$ ($r = 0.983$, $p << 0.001$, $R^2 = 0.965$), and $VSV^{soft+bone}_{weighted}$ ($r = 1.000$, $p << 0.001$, $R^2 = 0.999$).

The Bland-Altman plots in Figure 2 show low biases compared to MC for the absorbed bone lesion dose estimates achieved with the density weighted $VSV^{soft}_{weighted}$ and $VSV^{soft+bone}_{weighted}$. Furthermore, their corresponding limits of agreement were the smallest with fewest outliers of all investigated methods. Figure 3 visualizes a patient example showing the same sagittal slice of 3D voxel absorbed dose maps from the 3D dosimetry methods fused with the corresponding image slice of the patient`s CT (Figure 3 b). The 3D absorbed dose maps for bone lesions obtained from MC (Figure 3 a), $VSV^{soft}_{weighted}$ (Figure 3 d), and $VSV^{soft+bone}_{weighted}$ (Figure 3 f) are comparable. The 3D absorbed dose map of VSV^{soft} (Figure 3 c) generally overestimates and $VSV^{soft+bone}$ (Figure 3 e) underestimates the 3D absorbed dose map obtained from MC (Figure 3 a).

The cumulative DVH shown in Figure 4 represents the percentage of the volume receiving at least a certain absorbed dose in the VOI for one randomly chosen bone lesion. The curves of the $VSV^{soft}_{weighted}$ and $VSV^{soft+bone}_{weighted}$ methods show the highest concordance with the reference MC method. In contrast, without weighting, $VSV^{soft+bone}$ shows an underestimation and VSV^{soft} an overestimation of absorbed doses. Vertical red lines represent the OLINDA and $OLINDA_{weighted}$ absorbed dose estimates for the lesion, and the horizontal and vertical black line represent the percentage of volume receiving the mean absorbed lesion dose estimate from MC simulation. Similar to the VSV^{soft} approach, the OLINDA method yields higher values compared to the mean MC lesion absorbed dose. With applied density weighting, $OLINDA_{weighted}$ underestimates the absorbed lesion dose estimate. This provides a closer look at why the results shown in Figure 1 and Figure 2 are following those trends.

Discussion

Patients with advanced mCRPC often present with a significantly high tumor burden in the bone. Furthermore, osteosclerotic bone metastases can develop an increased number of osteoblasts leading to an elevated bone mass and increased density in the bone lesions (29). Consequently, bone lesion absorbed dose estimates in Lu-177-PSMA therapy are affected by regional variations in bone tissue density, and the accuracy of computed dose estimates may significantly depend on the

capability of the dosimetry method of choice to account for these local changes. In this study, different techniques for VOI-wise and 3D voxel-wise dosimetry with varying complexity and practicability were compared. Simplified methods with reduced complexity were tested against dose estimation by full Monte Carlos simulation. The latter served as reference standard, since it inherently accounts for local differences in activity distribution and tissue density changes in the individual patient. For this purpose, dosimetry results of 289 bone lesions of 15 mCRPC patients receiving their first cycle of Lu-177-PSMA-I&T therapy were assessed. To our knowledge, this study is the first approach to analyze and compare varying dosimetric approaches for dose estimation in a high number of bone lesions in Lu-177-PSMA therapy. However, accurate, personalized tumor dosimetry is mandatory for patient tailored approaches to increase tumor doses and thus improvement of patient outcome, to examine dose response relationships and to build predictive models for therapy outcomes. Moreover, our results have the potential to enable a comparability of published absorbed doses in bone lesions from different authors using different dosimetry methods.

The first method being investigated was based on the classical application of OLINDA/EXM®, which is widely clinically available and has been commonly used for dosimetry estimations in Lu-177-PSMA therapies (5-7, 9-11). However, our results indicate that OLINDA bone lesion absorbed doses have a wide variation when compared to MC. The percentage deviations of absorbed lesion doses compared to the reference MC dose ranged from an underestimation of -60 % to an overestimation by +47 %, yielding a mean overestimation of +7 ±13 % in all lesions. This broad range of deviations can partly be explained by the different assumptions made within this approach: the tumor is of a spherical shape, the activity distribution is uniform, and the tumor is of unit density. The various different densities of bone lesions may have the greatest impact. Howard et al. (30) compared lesion absorbed dose estimates from OLINDA sphere model against MC simulation for Iodine-131 (I-131) radioimmunotherapy of lymphoma patients and concluded that the lesion shape has a minor impact when comparing the self-dose component. Their investigations revealed a dose underestimation compared to MC dose with a range of percentage deviations from -2 % to -31 %. Grimes et al. (18)

found good agreement of neuroendocrine tumor absorbed doses for Lu-177 from the OLINDA sphere model and MC simulations with average deviations smaller than -3.5 % ± 5.1 %. Similar results with differences smaller than -5 % were found by Divoli et al. (31), comparing absorbed doses of OLINDA and MC for artificial spherical tumors in liver and lung. These publications addressed soft tissue lesions with relatively comparable densities.

In contrast, this work focusses on the estimation of the absorbed dose in bone lesions with varying intra-lesion density. Introducing the VOI-based method $OLINDA_{weighted}$, we hence attempted to correct for the different density of bone lesions compared to the OLINDA unit density sphere model by using the average lesion density obtained from the patient's CT scan. This approach resulted in a reduction of the spread of the PD of absorbed dose estimates (min: -54 %; max: -2 %) but led to an average dose underestimation of -15 ±6 %, in contrast to the dose overestimation of +7 ±13 % (min: -60 %; max: +47 %) observed with the unaltered OLINDA method without subsequent density weighting. Our proposed $OLINDA_{weighted}$ dosimetry method prevents absorbed tumor dose overestimation. To the best of our knowledge, density weighting approaches applied to the OLINDA framework in bone lesions are not found in the literature. We recommend a density weighting as proposed in our work for future investigations, since we observed a risk of overestimating tumor absorbed doses by assuming a soft tissue density in bone lesions in our investigations.

The 3D dosimetry approach for Lu-177-PSMA therapy recently published by Violet et al. (8) reported the application of an ICRP soft tissue voxel dose kernel for deriving absorbed dose estimates for organs and tumors in lymph nodes and bone lesions. In our present work, we further investigated the utilization of VSVs for bone lesion dosimetry by direct comparison with the Monty Carlo dose simulation as the reference standard. Based on our results for 3D absorbed dose calculations, we observed that both approaches, the utilization of singular soft tissue VSVs (VSV^{soft}) and of separate VSVs for soft tissue and bone ($VSV^{soft+bone}$), reveal limitations in accurate estimation of absorbed dose in bone lesions. While on average VSV^{soft} demonstrated a strong overestimation by +16 ±13 % (min: -56 %; max: +57 %), $VSV^{soft+bone}$ on the other hand still showed limited capability of adequately

estimating the absorbed dose in each individual bone lesion, it exhibited a large underestimation of absorbed dose by -35 ±8 % (min: -76 %; max: +5 %). These observations may be explained by the underestimated tissue density, which is an inherent characteristic of the soft tissue voxel dose kernel VSV^{soft}, compared to the actual bone lesion density. Therefore, this underestimation of voxel density results in an underestimation of the voxel's mass and consequently in an overestimation of the absorbed dose, which is the deposited energy per unit mass. On the other hand, $VSV^{soft+bone}$ relies on the assumption that bone lesions consist merely out of cortical bone, although a typical bone lesion has different components and densities (32). In this case, a larger mass than the actual lesion mass is assumed, and consequently the observed absorbed dose is artificially smaller.

So far, dosimetry calculations using VSVs were mainly applied in settings with heterogeneous activity distributions in homogeneous density distributions. For these implementations, a high agreement for tumor absorbed doses obtained from VSVs for soft tissue and MC simulation for soft tissue lesions was reported. Grimes et al. (18) reported only -1.5 % ± 4.6 % difference for Lu-177 and Dieudonné et al. (33) stated -0.33 % difference for Yttrium-90 (Y-90) and -0.15 % difference for I-131 for a hepatic tumor phantom. In general, VSVs dosimetry calculations can account for heterogeneous activity distributions but not for density differences since they were simulated for a single homogeneous medium. For the majority of organs and lesions in the abdomen, only small density variations are assumed and a VSV^{soft} approach can therefore be safely used in the clinical setting. However, the above mentioned assumption has to be questioned in situations with significantly large local tissue density changes. Especially for bone lesions in mCRPC patients, the lesion densities can vary to a large extent, on average and per voxel. Therefore, a dosimetry calculation method needs to address these density changes and an adapted dose estimation approach becomes mandatory.

The VSV dosimetry methods with subsequent density weighting, as investigated in our study, seem to better address voxel-wise density changes, and may therefore yield to improved absorbed lesion dose estimate agreements with MC simulation. The proposed methods $VSV^{soft}_{weighted}$ and $VSV^{soft+bone}_{weighted}$ expressed significantly reduced deviations of estimated lesion dose compared to the reference

Monte Carlo simulation, with an underestimation of on average -5 ±2 % (min: -15 %; max: -2 %) and -3 ±2 % (min: -13 %; max: 0 %), respectively. This observation is in concordance with Dieudonné et al. (17), who reported improved dose agreement for a density corrected VSV approach compared to full MC 3D dosimetry for three clinical cases with focus on soft tissue. Dieudonné et al. observed a lesion absorbed dose difference for a I-131-Tositumomab case of -3.1 %, an organ absorbed dose difference of maximum -1.1 % for a Lu-177-peptide case and an organ absorbed dose difference of maximum + 0.8 % for a Y-90-microspheres case. Besides, Lee et al. (27) noted an overall improvement of whole-body dose estimates when introducing multiple tissue-specific VSVs, when compared to the utilization of a single tissue VSV. However, out results for bone lesion dosimetry indicate that the effect of additional density weighting onto a single VSV ($VSV^{soft}_{weighted}$ compared to VSV^{soft}) outperformed the effect of adding multiple VSVs for various tissues without density weighting ($VSV^{soft+bone}$ compared to VSV^{soft}).

The advantage of 3D absorbed dose maps generated by VSV or MC approaches is obviously the visualization of lesion regions receiving higher or lower absorbed doses on a voxel level. The investigated VSV dosimetry methods as well as the MC simulation provide 3D absorbed dose maps, while the OLINDA dosimetry methods are losing the distribution information. Cumulative DVHs accompanying 3D absorbed dose distribution maps may provide detailed information of regional lesion absorbed dose estimates. Individual voxels might potentially be influenced by image artifacts and hence have an impact on the shape of the DVH. Consequently, DVHs should be interpreted cautiously. The exemplarily DVH in Figure 4 furthermore confirms the finding that the curves of weighted VSV dosimetry approaches show a dose distribution closest to the one of full MC dosimetry simulation.

Regarding the simplicity and ease to use, the OLINDA unit density sphere method is superior to the other investigated dosimetry methods in this study. On the other hand, with respect to the accuracy, the MC absorbed dose simulation is superior to all alternative approaches. However, at the same time it is the most complex method because of the requirement of additional pre- and post-

processing steps, and additional approximately 4.5 h MC simulation time in our investigation. This limits the use in clinical routine and this approach is likely to remain an in-house solution for research purposes and a tool for developing, evaluating and establishing approaches with increased applicability and usability. However, first approaches of using commercially available software solutions with VSVs for different radionuclide therapies have already been presented, see Maughan et al. (34), Kafrouni et al. (35). For bone lesion dosimetry in Lu-177-PSMA therapy, our results suggest that adding the density correction to the VSV based dosimetry approaches provides similar results to MC. Consequently, this proposed method may become a suitable and applicable clinical tool for combined soft tissue and bone lesion dosimetry in Lu-177-PSMA therapy.

To make tumor dosimetry widely available in clinical routine, ideally an existing software approach would be preferred. Furthermore, it needs to be adaptable to existing software and workflows in clinics, which can range from OLINDA/EXM® to customized in-house solutions. With our investigation and results for Lu-177-PSMA bone lesion dosimetry, we aimed at providing an estimate for the accuracy of the different tested dosimetry methods and the possible range of deviations. We are aware that the proposed density weighting approaches require an implementation into existing dosimetry solutions in an institute or clinic. However, this is justified by the improved accuracy of absorbed dose estimates demonstrated by our results.

Besides the minimization of absorbed radiation dose to organs at risk, routinely performed tumor dosimetry in Lu-177-PSMA therapy of mCRPC patients is important to improve patients' outcome. By increasing the accuracy of the personalized dosimetry estimates, a deeper understanding of therapy response could be achieved. Furthermore, our results facilitate the inter-center comparability of reported bone lesion dose estimates.

Conclusions

In our study of 289 bone lesions in mCRPC patients receiving Lu-177-PSMA-I&T therapy, the proposed voxel S value dosimetry approach with subsequent density weighting was associated with

comparable absorbed dose estimates for bone lesions as obtained with full patient-individual Monte Carlo dosimetry simulation. Density-weighted voxel S value dosimetry may provide accurate and reproducible tissue and bone-lesion dose estimation at tremendously reduced time and effort compared to full MC simulation. It therefore has the potential to enable routine therapy response evaluations.

List of abbreviations

mCRPC: metastatic, castration-resistant prostate carcinoma; PMSA: prostate-specific membrane antigen; Lu-177: Lutetium-177; OAR: organ at risk; VSV: voxel S value; 3D: three-dimensional; MC: Monte Carlo; p.i.: post injection; MELP: medium-energy low-penetration; VOI: volume of interest; HU: Hounsfield Unit; MIRD: Medical Internal Radiation Dose; ICRP: International Commission On Radiological Protection; PD: percentage difference; DVH: dose volume histogram; I-131: Iodine-131; Y-90: Yttrium-90

Declaration

Ethics approval and consent to participate

This study is based on retrospective and anonymized data, which was acquired for routine clinical dosimetry (Ethics Committee of LMU Munich 20-520).

Consent for publication

Not applicable.

Availability of data and material

Please contact author for data requests.

Funding

This work was partly funded by the German Research Foundation (DFG) within the Research Training Group GRK 2274.

Authors' contributions

JB, CU, AG, LK, AT, HI, PB, AR, AC, SZ and GB designed the concept of the study. FG was responsible for the radiopharmaceutical production. JB, AG, AT, HI, GB reviewed the clinical data for dosimetry. All data analysis was carried out by JB, CU, AG, GB. All authors contributed to the drafting of the manuscript, and all authors read and approved the manuscript.

Acknowledgements

We would like to thank Dr. François Bénard for facilitating the collaboration between LMU and BC Cancer (Vancouver, Canada). Special thanks to all technicians at the Department of Nuclear Medicine, University Hospital, LMU Munich for their participation in data collection.

Competing interests

The authors declare that they have no conflict of interest.

462 **Tables**

Patient	Age	Activity [GBq]	PSA [ng/ml] prior to therapy	Gleason score	Previous treatment				
					OP	RTx	AHT	CTx	Ra-223
1	61	7.44	25.9	9	0	1	1	1	0
2	75	7.46	38.4	9	1	0	1	1	0
3	75	7.44	1070	8	1	1	1	1	1
4	78	9.04	570	9	0	0	1	1	0
5	62	7.47	848	-	0	1	1	0	0
6	59	7.47	5.38	7b	0	1	1	1	0
7	74	9.19	1696	-	1	1	1	0	0
8	63	7.46	149	8	0	1	1	1	0
9	82	7.44	20.2	9	1	1	1	0	0
10	70	7.42	127	9	1	1	1	1	1
11	75	9.05	436	9	0	1	1	1	0
12	49	9.00	121	9	1	1	1	1	1
13	64	7.47	1268	8	0	1	1	1	0
14	79	7.46	72.7	7b	0	0	1	0	0
15	73	9.04	19.6	9	1	0	1	1	0

463 **Table 1.** Summary of patients being included. Previous treatment (1: yes; 0: no): OP surgery, RTx
464 radiotherapy, AHT anti-hormonal therapy (including second line AHT with bicalutamide,
465 enzalutamide, abiraterone acetate), CTx chemotherapy (docetaxel, cabazitaxel), Ra-223 radium-223
466 dichloride.

467

Method	OLINDA	$OLINDA_{weighted}$	VSV^{soft}	$VSV^{soft}_{weighted}$	$VSV^{soft+bone}$	$VSV^{soft+bone}_{weighted}$
Mean PD ±SD	7 ±13 %	-15 ±6 %	16 ±13 %	-5 ±2 %	-35 ±8 %	-3 ±2 %
Minimum PD	-60 %	-54 %	-56 %	-15 %	-76 %	-13 %
Maximum PD	47 %	-2 %	57 %	-2 %	5 %	0 %

468 **Table 2.** Percentage deviation (PD) with standard deviation (SD) of absorbed dose to bone lesions
469 compared to the reference MC absorbed dose estimate: averaged deviation over all lesions,
470 minimum and maximum deviation per lesion.

Figures

Figure 1. Percentage difference per bone lesion compared to the reference MC dose simulation.

Figure 2. Bland-Altman plots of lesion-wise dose estimates from each method, compared against the MC absorbed dose simulation.

Figure 3. Patient example showing the same sagittal slice of 3D absorbed dose maps, fused with the patient's CT image in (b). Maps in units of Gy/GBq were achieved with methods: MC (a), VSV^{soft} (c), $VSV^{soft}_{weighted}$ (d), $VSV^{soft+bone}$ (e), and $VSV^{soft+bone}_{weighted}$ (f).

Figure 4. Exemplary cumulative DVH for a bone lesion with 80.4 ml volume, the therapy activity was 9.044 GBq. The vertical red lines represent the absorbed lesion dose from the OLINDA and $OLINDA_{weighted}$ method. The horizontal and vertical black line represent the percentage of volume receiving the mean absorbed lesion dose from MC simulation.

References

1. Torre LA, Siegel RL, Ward EM, Jemal A. Global cancer incidence and mortality rates and trends—an update. Cancer Epidemiology and Prevention Biomarkers. 2016;25(1):16-27.
2. Zhou CK, Check DP, Lortet-Tieulent J, Laversanne M, Jemal A, Ferlay J, et al. Prostate cancer incidence in 43 populations worldwide: an analysis of time trends overall and by age group. International journal of cancer. 2016;138(6):1388-400.
3. Gosewisch A, Ilhan H, Tattenberg S, Mairani A, Parodi K, Brosch J, et al. 3D Monte Carlo bone marrow dosimetry for Lu-177-PSMA therapy with guidance of non-invasive 3D localization of active bone marrow via Tc-99m-anti-granulocyte antibody SPECT/CT. EJNMMI Research. 2019;9(1):76.
4. Kratochwil C, Fendler WP, Eiber M, Baum R, Bozkurt MF, Czernin J, et al. EANM procedure guidelines for radionuclide therapy with 177 Lu-labelled PSMA-ligands (177 Lu-PSMA-RLT). European journal of nuclear medicine and molecular imaging. 2019;46(12):2536-44.
5. Delker A, Fendler WP, Kratochwil C, Brunegraf A, Gosewisch A, Gildehaus FJ, et al. Dosimetry for 177 Lu-DKFZ-PSMA-617: a new radiopharmaceutical for the treatment of metastatic prostate cancer. European journal of nuclear medicine and molecular imaging. 2016;43(1):42-51.
6. Okamoto S, Thieme A, Allmann J, D'Alessandria C, Maurer T, Retz M, et al. Radiation dosimetry for 177Lu-PSMA I&T in metastatic castration-resistant prostate cancer: absorbed dose in normal organs and tumor lesions. Journal of Nuclear Medicine. 2017;58(3):445-50.
7. Fendler WP, Reinhardt S, Ilhan H, Delker A, Böning G, Gildehaus FJ, et al. Preliminary experience with dosimetry, response and patient reported outcome after 177Lu-PSMA-617 therapy for metastatic castration-resistant prostate cancer. Oncotarget. 2017;8(2):3581.
8. Violet J, Jackson P, Ferdinandus J, Sandhu S, Akhurst T, Iravani A, et al. Dosimetry of 177Lu-PSMA-617 in metastatic castration-resistant prostate cancer: correlations between pretherapeutic imaging and whole-body tumor dosimetry with treatment outcomes. Journal of Nuclear Medicine. 2019;60(4):517-23.
9. Baum RP, Kulkarni HR, Schuchardt C, Singh A, Wirtz M, Wiessalla S, et al. Lutetium-177 PSMA radioligand therapy of metastatic castration-resistant prostate cancer: safety and efficacy. Journal of Nuclear Medicine. 2016:jnumed. 115.168443.
10. Kratochwil C, Giesel FL, Stefanova M, Benešová M, Bronzel M, Afshar-Oromieh A, et al. PSMA-targeted radionuclide therapy of metastatic castration-resistant prostate cancer with 177Lu-labeled PSMA-617. Journal of Nuclear Medicine. 2016;57(8):1170-6.
11. Yadav MP, Ballal S, Tripathi M, Damle NA, Sahoo RK, Seth A, et al. Post-therapeutic dosimetry of 177Lu-DKFZ-PSMA-617 in the treatment of patients with metastatic castration-resistant prostate cancer. Nuclear medicine communications. 2017;38(1):91-8.
12. Stabin MG, Sparks RB, Crowe E. OLINDA/EXM: the second-generation personal computer software for internal dose assessment in nuclear medicine. Journal of nuclear medicine. 2005;46(6):1023-7.
13. Bolch WE, Bouchet LG, Robertson JS, Wessels BW, Siegel JA, Howell RW, et al. MIRD pamphlet no. 17: the dosimetry of nonuniform activity distributions—radionuclide S values at the voxel level. Journal of Nuclear Medicine. 1999;40(1):11S-36S.
14. Sohlberg A, Watabe H, Iida H. Acceleration of Monte Carlo-based scatter compensation for cardiac SPECT. Physics in Medicine & Biology. 2008;53(14):N277.
15. Kangasmaa T, Sohlberg A, Kuikka JT. Reduction of collimator correction artefacts with bayesian reconstruction in spect. International journal of molecular imaging. 2011;2011.
16. Schneider W, Bortfeld T, Schlegel W. Correlation between CT numbers and tissue parameters needed for Monte Carlo simulations of clinical dose distributions. Physics in Medicine & Biology. 2000;45(2):459.
17. Dieudonné A, Hobbs RF, Lebtahi R, Maurel F, Baechler S, Wahl RL, et al. Study of the impact of tissue density heterogeneities on 3-dimensional abdominal dosimetry: comparison between dose kernel convolution and direct Monte Carlo methods. Journal of Nuclear Medicine. 2013;54(2):236-43.

18. Grimes J, Celler A. Comparison of internal dose estimates obtained using organ-level, voxel S value, and Monte Carlo techniques. Medical physics. 2014;41(9):092501.
19. Papadimitroulas P. Dosimetry applications in GATE Monte Carlo toolkit. Physica Medica. 2017;41:136-40.
20. Papadimitroulas P, Loudos G, Nikiforidis GC, Kagadis GC. A dose point kernel database using GATE Monte Carlo simulation toolkit for nuclear medicine applications: Comparison with other Monte Carlo codes. Medical physics. 2012;39(8):5238-47.
21. Sarrut D, Bardiès M, Boussion N, Freud N, Jan S, Létang JM, et al. A review of the use and potential of the GATE Monte Carlo simulation code for radiation therapy and dosimetry applications. Medical physics. 2014;41(6Part1).
22. Chetty IJ, Rosu M, Kessler ML, Fraass BA, Ten Haken RK, McShan DL. Reporting and analyzing statistical uncertainties in Monte Carlo–based treatment planning. International Journal of Radiation Oncology* Biology* Physics. 2006;65(4):1249-59.
23. Snyder W, Ford M, Warner G, Watson S. MIRD pamphlet no. 11. The Society of Nuclear Medicine, New York. 1975:92-3.
24. Lassmann M, Chiesa C, Flux G, Bardiès M. EANM Dosimetry Committee guidance document: good practice of clinical dosimetry reporting. European journal of nuclear medicine and molecular imaging. 2011;38(1):192-200.
25. NIST National Institute of Standards and Technonolgy. https://physics.nist.gov/cgi-bin/Star/compos.pl. Accessed 21 July 2020.
26. McConn RJ, Gesh CJ, Pagh RT, Rucker RA, Williams III R. Compendium of material composition data for radiation transport modeling. Pacific Northwest National Lab.(PNNL), Richland, WA (United States); 2011.
27. Lee MS, Kim JH, Paeng JC, Kang KW, Jeong JM, Lee DS, et al. Whole-body voxel-based personalized dosimetry: the multiple voxel S-value approach for heterogeneous media with nonuniform activity distributions. Journal of Nuclear Medicine. 2018;59(7):1133-9.
28. Bland JM, Altman DG. Statistical methods for assessing agreement between two methods of clinical measurement. International Journal of Nursing Studies. 2010;47(8):931-6.
29. Ibrahim T, Flamini E, Mercatali L, Sacanna E, Serra P, Amadori D. Pathogenesis of osteoblastic bone metastases from prostate cancer. Cancer: Interdisciplinary International Journal of the American Cancer Society. 2010;116(6):1406-18.
30. Howard DM, Kearfott KJ, Wilderman SJ, Dewaraja YK. Comparison of I-131 radioimmunotherapy tumor dosimetry: unit density sphere model versus patient-specific Monte Carlo calculations. Cancer Biotherapy and radiopharmaceuticals. 2011;26(5):615-21.
31. Divoli A, Chiavassa S, Ferrer L, Barbet J, Flux GD, Bardies M. Effect of patient morphology on dosimetric calculations for internal irradiation as assessed by comparisons of Monte Carlo versus conventional methodologies. Journal of Nuclear Medicine. 2009;50(2):316-23.
32. Hough M, Johnson P, Rajon D, Jokisch D, Lee C, Bolch W. An image-based skeletal dosimetry model for the ICRP reference adult male—internal electron sources. Physics in Medicine & Biology. 2011;56(8):2309.
33. Dieudonné A, Hobbs RF, Bolch WE, Sgouros G, Gardin I. Fine-resolution voxel S values for constructing absorbed dose distributions at variable voxel size. Journal of nuclear medicine. 2010;51(10):1600-7.
34. Maughan NM, Garcia-Ramirez J, Arpidone M, Swallen A, Laforest R, Goddu SM, et al. Validation of post-treatment PET-based dosimetry software for hepatic radioembolization of Yttrium-90 microspheres. Medical physics. 2019;46(5):2394-402.
35. Kafrouni M, Allimant C, Fourcade M, Vauclin S, Delicque J, Ilonca A-D, et al. Retrospective voxel-based dosimetry for assessing the ability of the body-surface-area model to predict delivered dose and radioembolization outcome. Journal of Nuclear Medicine. 2018;59(8):1289-95.

Figures

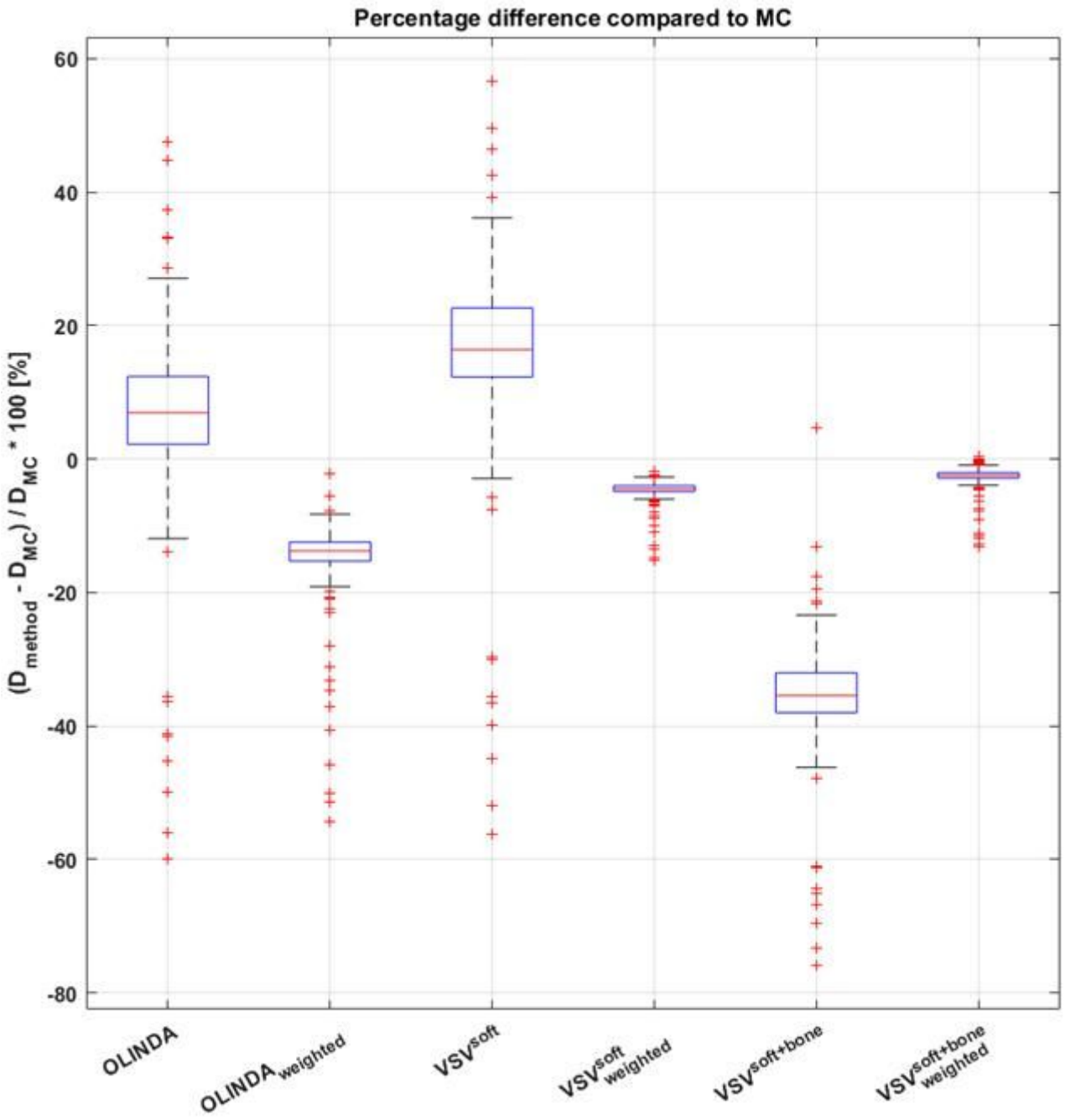

Figure 1

Percentage difference per bone lesion compared to the reference MC dose simulation.

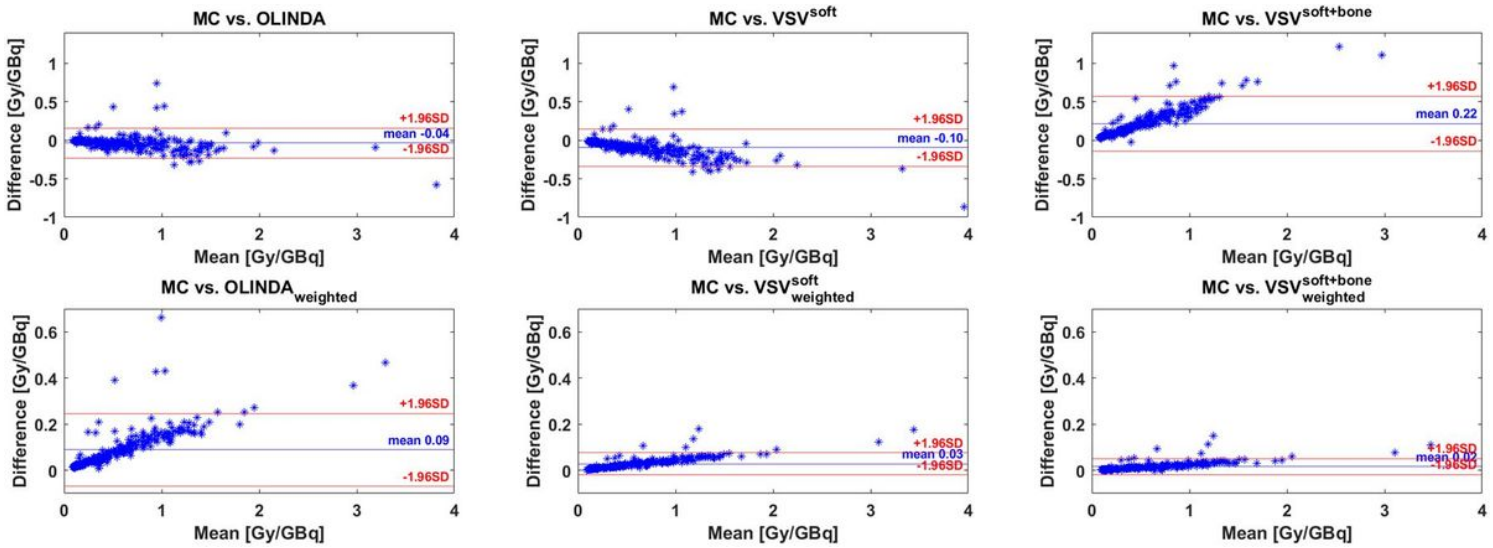

Figure 2

Bland-Altman plots of lesion-wise dose estimates from each method, compared against the MC absorbed dose simulation.

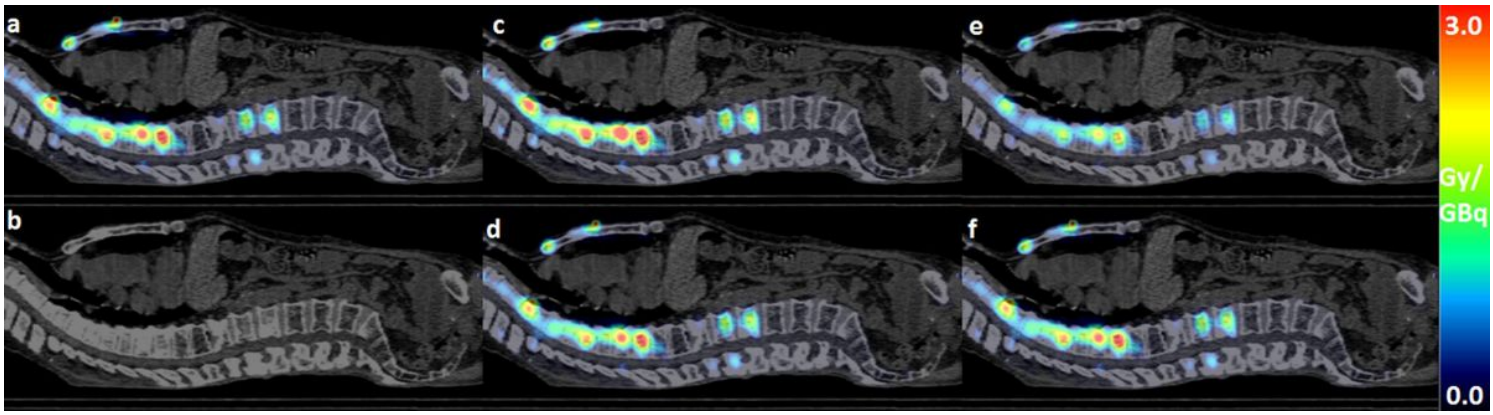

Figure 3

Patient example showing the same sagittal slice of 3D absorbed dose maps, fused with the patient's CT image in (b). Maps in units of Gy/GBq were achieved with methods: MC (a), VSVsoft (c), (d), VSVsoft+bone (e), and (f).

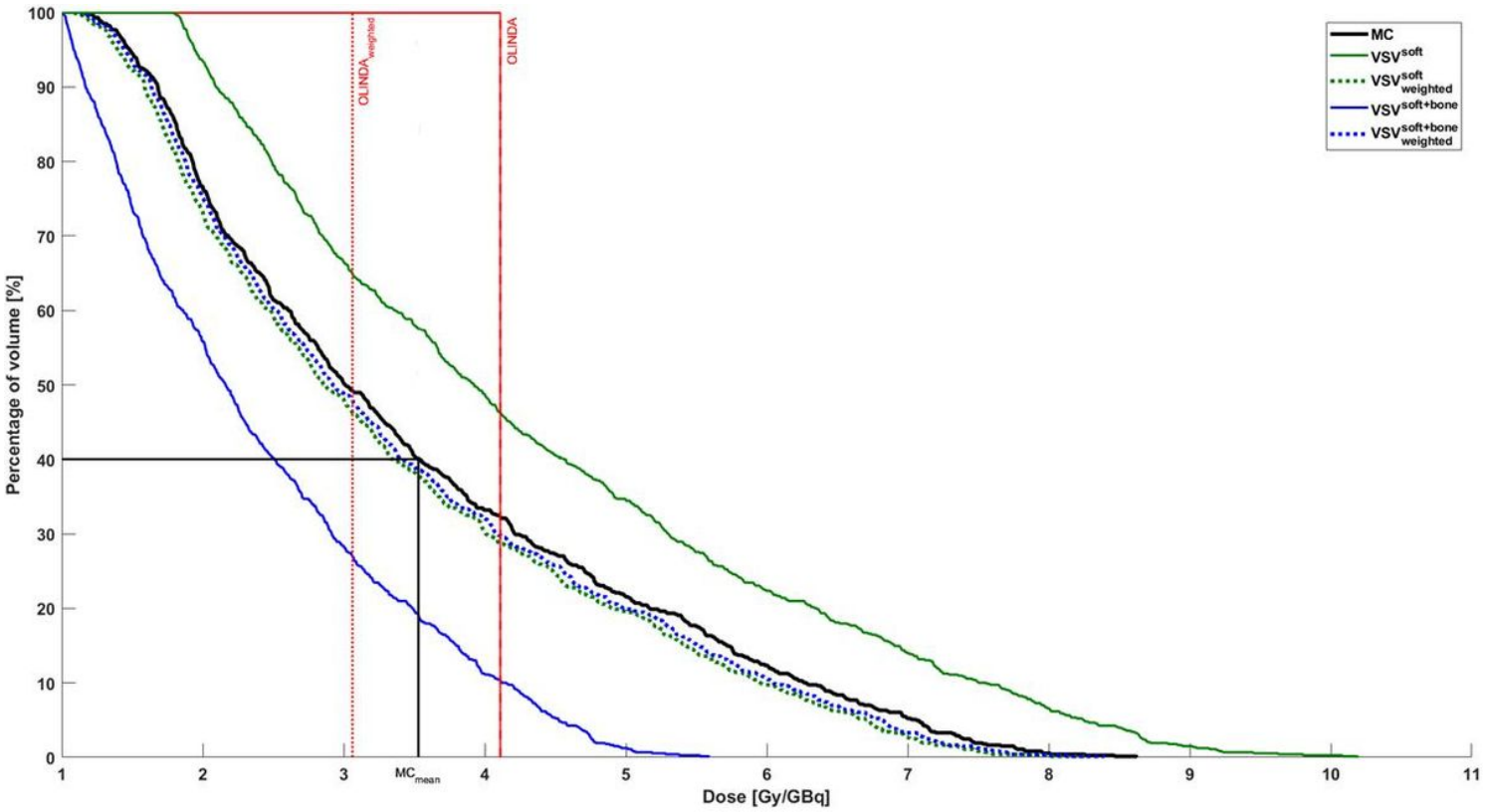

Figure 4

Exemplary cumulative DVH for a bone lesion with 80.4 ml volume, the therapy activity was 9.044 GBq. The vertical red lines represent the absorbed lesion dose from the OLINDA and OLINDAweighted method. The horizontal and vertical black line represent the percentage of volume receiving the mean absorbed lesion dose from MC simulation.